J. Fluid Mech. (2025), *vol.* 1019, A6, doi:10.1017/jfm.2025.10573

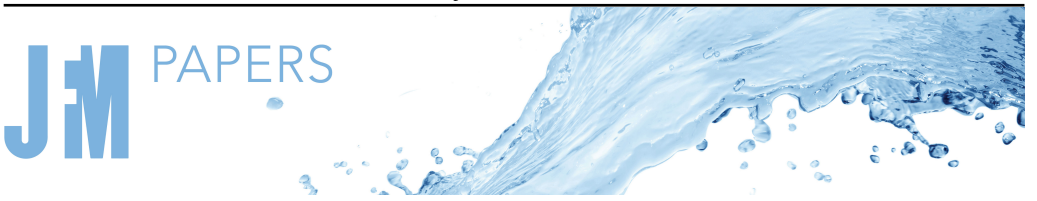

Coastal wave refraction in variable currents over a varying bathymetry

Trygve Halsne[1] **and Yan Li**[2]

[1]Norwegian Meteorological Institute, N-5007 Bergen, Norway

[2]Department of Mathematics, University of Bergen, N-5007 Bergen, Norway

Corresponding author: Trygve Halsne, trygveh@met.no

(Received 14 January 2025; revised 12 August 2025; accepted 14 August 2025)

Refraction is the predominant mechanism causing spatially inhomogeneous surface gravity wave fields. However, the complex interplay between depth- and current-induced wave refraction remains poorly understood. Assuming weak currents and slowly varying bathymetry, we derive an analytical approximation to the wave ray curvature, which is validated by an open-source ray tracing framework. The approximation has the form of linear superposition of a current- and a depth-induced component, each depending on the gradients in the ambient fields. This separation enables quantification of their individual and combined contributions to refraction. Through analysis of a few limiting cases, we demonstrate how the sign and magnitude of these components influence the wave refraction, and identify conditions where they either amplify or counteract each other. We also identify which of the two plays a dominant role. These findings provide physically resolved insights into the influence of current and depth gradients on wave propagation, and are relevant for applications related to remote sensing and coastal wave forecasting services.

Key words: coastal engineering, surface gravity waves, wave scattering

1. Introduction

Refraction is a key mechanism modulating the surface gravity wave field. For example, the horizontal wave field variability in deep waters is dictated by current-induced refraction (Ardhuin *et al.* 2017; Bôas *et al.* 2020) – a mechanism that also influences the occurrence probability of so-called freak waves (Smith 1976; White & Fornberg 1998; Hjelmervik & Trulsen 2009; Onorato, Proment & Toffoli 2011). Most human marine activities take place in the coastal or near-coastal zone. Such regions are often classified as intermediate

or shallow with respect to a characteristic wavelength. As a consequence, the wave propagation is typically accompanied by variable currents and varying bathymetry, which can give rise to hazardous sea states (Halsne *et al.* 2022; Li & Chabchoub 2023; Zheng, Li & Ellingsen 2023).

Under the geometric optics approximation, wave action density propagates along wave rays (Whitham 1965). An appropriate measure of wave refraction is the ray curvature, which in plain language means the departure from a straight line. Approximate ray curvature solutions have been derived for conditions with either depth- or current-induced refraction (Arthur, Munk & Isaacs 1952; Kenyon 1971; Dysthe 2001), where the latter was first derived by Landau & Lifshitz (1987, Ch. 3, § 68) for sound waves. These have provided valuable insights into where wave refraction becomes important and where to expect modulations, both local and non-local, of the wave field (e.g. Gallet & Young 2014; Quilfen *et al.* 2018; Bôas *et al.* 2020). Under mixed conditions, when both a varying current and bathymetry are present, the analysis is typically carried out through direct numerical integration of the wave ray equations (e.g. Arthur 1950; Jonsson & Wang 1980; Romero, Hypolite & McWilliams 2020; Halsne *et al.* 2022), where it remains physically unresolved as to how the two play a joint role in the wave refraction. The purpose of this work is to develop a theoretical model that elucidates this interplay.

Knowledge about where, and under which conditions, one might expect strong wave–current–depth interactions is considered valuable information for various geophysical applications. For instance, in recent decades there has been an increased focus on retrieving current or bathymetry information using remote sensing observations of the spatially varying wave field (see e.g. Stewart & Joy 1974; Hessner *et al.* 2014; Lund *et al.* 2015; Smeltzer *et al.* 2019; Lenain *et al.* 2023; Klotz *et al.* 2024). Furthermore, recent work shows that a prescribed mean flow field can be used to map the horizontal wave height variability in deep waters, by taking into account the directional diffusion of wave action caused by current-induced refraction (Smit & Janssen 2019; Bôas & Young 2020; Wang *et al.* 2023). In water regions where both a varying current and bathymetry are present, the development of remote sensing techniques and simplified prediction models is based on an explicit representation of how the current and bathymetry play a role in modulating the wave field. In this context, approximate solutions serve as adequate alternatives to complex exact solutions (see e.g. Phillips 1977; Lavrenov 2003; Mei, Stiassnie & Yue 2005) for analysing wave–current–depth interactions.

How wave fields are altered by their ambient environments in the presence of both a varying current and bathymetry remains an open research question. Hence, the main objective of this work is to address this question by developing a simplified theoretical model accounting for the combined effects of varying current and bathymetry on wave refraction. The main focus is therefore on the wave kinematics and not the dynamics. This paper is laid out as follows: we first derive an analytical approximation to the curvature of wave rays in § 2 under the weak current assumption and geometric optics approximation. Then, the complex interplay between current- and depth-induced refraction is explored in a few limiting cases, by utilising an open-source ray tracing framework (§ 3). Finally, the conclusions are drawn in § 4.

2. Wave ray theory

We consider three-dimensional surface waves atop a background current and a varying bathymetry, assuming incompressible and inviscid flows. A still water surface is considered at the vertical axis $z = 0$ in the horizontal x–y plane. Let $\boldsymbol{U} = [U_1(t, \boldsymbol{x}), U_2(t, \boldsymbol{x})]$ be the velocity vector of the background current in the horizontal

plane with $\boldsymbol{x} = (x, y)$ the position vector in a fixed coordinate system, U_1 and U_2 the velocity component in the x- and y-directions, respectively. The velocity vector $\boldsymbol{U}$ is assumed to be depth uniform, and slowly dependent on the time t and $\boldsymbol{x}$ compared with the rapidly varying phase of the surface waves. A water depth $h(\boldsymbol{x})$, is considered, which varies mildly in the horizontal plane.

Let $\theta(\boldsymbol{x}, t)$ be the wave phase, such that

$$\nabla\theta = \boldsymbol{k},\ \partial_t\theta = -\omega, \quad \text{and} \quad \partial_t\boldsymbol{k}(\boldsymbol{x}, t) + \nabla\omega(\boldsymbol{x}, t) = 0, \tag{2.1a,b,c}$$

by definition. Here, $\nabla = (\partial_x, \partial_y)$; $\boldsymbol{k}$ and ω denote the local wave vector and angular frequency of waves, which are modified by the presence of both current and varying bathymetry, obeying the dispersion relation as follows (Peregrine 1976):

$$\omega(\boldsymbol{k}, \boldsymbol{x}) = \boldsymbol{k}\cdot\boldsymbol{U} + \Omega(k, \boldsymbol{x}), \tag{2.2}$$

where $\Omega(k, \boldsymbol{x}) = \sqrt{gk\tanh kh(\boldsymbol{x})}$ denotes the intrinsic wave frequency in the absence of currents, g is the gravitational acceleration, and $k = |\boldsymbol{k}|$ denotes the magnitude of the wave vector. For convenience and later reference, we introduce the group velocity vector and phase velocity associated with the intrinsic wave frequency as follows, respectively,

$$\boldsymbol{c}_g(\boldsymbol{k}, \boldsymbol{x}) = \nabla_k\Omega \quad \text{and} \quad c(k, \boldsymbol{x}) = \Omega/k, \tag{2.3a,b}$$

where the operator $\nabla_k = (\partial_{k_x}, \partial_{k_y})$ denotes the gradient in the $\boldsymbol{k}$ space.

2.1. *Rays and their unit tangent vector*

Wave rays are time dependent and described as position vectors in the horizontal plane, denoted by $\boldsymbol{r} = [x_r(t), y_r(t)]$. Here, the subscript '$r$' is used to distinguish it from the position vector $\boldsymbol{x} = (x, y)$ in the fixed Cartesian coordinate system. According to the definition (Mei *et al.* 2005,their § 3.6)

$$\frac{\mathrm{d}\boldsymbol{r}}{\mathrm{d}t} = \nabla_k\omega(\boldsymbol{k}, \boldsymbol{x}) \equiv \boldsymbol{U} + \boldsymbol{c}_g \quad \rightarrow \quad \frac{\mathrm{d}y_r}{\mathrm{d}x_r} = \frac{\dot{y}_r}{\dot{x}_r}, \tag{2.4a,b}$$

where the dot denotes the derivative with respect to t. Here, (2.4*a*) denotes the absolute group velocity vector and (2.4*b*) leads to the general expression for the local slope of the rays which will be used for the ray curvature presented in § 2.2. The definition of the rays has the physical meaning of wave group trajectories, i.e. the rays are locally parallel to the absolute group velocity everywhere at all times, and denote the direction of wave action propagation (Whitham 1965).

The material derivative of the wave vector $\mathrm{d}\boldsymbol{k}/\mathrm{d}t$ is obtained by the substitution of (2.2) into (2.1*c*), giving rise to

$$\partial_t\boldsymbol{k} + (\nabla_k\omega\cdot\nabla)\boldsymbol{k} + \nabla\omega = 0, \tag{2.5}$$

where $\omega = \omega(\boldsymbol{k}(\boldsymbol{x}, t), \boldsymbol{x})$ was used. Hence, the material derivative of the wave vector is defined as

$$\frac{\mathrm{d}\boldsymbol{k}}{\mathrm{d}t} \equiv \partial_t\boldsymbol{k} + (\nabla_k\omega\cdot\nabla)\boldsymbol{k}, \text{ and thus } \frac{\mathrm{d}\boldsymbol{k}}{\mathrm{d}t} = -\nabla\omega(\boldsymbol{k}, \boldsymbol{x}), \tag{2.6a,b}$$

according to (2.5). A different but equivalent definition for $\mathrm{d}\boldsymbol{k}/\mathrm{d}t$ was used in Landau & Lifshitz (1987), which would also lead to (2.6*b*).

The unit tangent vector of the rays $\boldsymbol{t}$, is essential to the explicit expression of the ray curvature, which can be obtained by noting that $(\mathrm{d}\boldsymbol{r}/\mathrm{d}t)/\!/\boldsymbol{t}$ and $|\boldsymbol{t}| = 1$, showing that the

following identities hold:

$$\boldsymbol{t} = \frac{\boldsymbol{U} + \boldsymbol{c}_g}{|\boldsymbol{U} + \boldsymbol{c}_g|} \quad \text{and} \quad \boldsymbol{t} = \left[\frac{\dot{x}_r}{\dot{s}}, \quad \frac{\dot{y}_r}{\dot{s}}\right], \tag{2.7a,b}$$

where $\dot{s} = |\dot{\boldsymbol{r}}| \equiv \sqrt{(\dot{x}_r)^2 + (\dot{y}_r)^2}$, and $s(t)$ denotes the arc length. Here, both the expressions will be used for the derivation of the ray curvature. The assumption of weak current compared with the group velocity of the waves is translated to the definition of the dimensionless current velocity as follows

$$\boldsymbol{u} = [u, v] = \boldsymbol{U}/c_g, \tag{2.8}$$

such that $\mathcal{O}(|\boldsymbol{u}|) \sim \varepsilon$, with $c_g = |\boldsymbol{c}_g|$, u and v representing the component of $\boldsymbol{u}$ in the x- and y-direction, respectively, and ε denoting a small dimensionless scaling parameter. Thus, the unit tangent vector given by (2.7*a*) can be expressed as

$$\boldsymbol{t} = \frac{\boldsymbol{u} + \boldsymbol{e}_k}{|\boldsymbol{u} + \boldsymbol{e}_k|} = \boldsymbol{e}_k + \boldsymbol{u} - (\boldsymbol{u} \cdot \boldsymbol{e}_k)\boldsymbol{e}_k + \mathcal{O}(\varepsilon^2), \tag{2.9}$$

where $\boldsymbol{e}_k = \boldsymbol{k}/k$ denotes the unit vector in the same direction as the local wave vector. The approximation to the unit tangent vector given by (2.9) is identical to Dysthe (2001, expression (3)) for the limiting cases of deep water waves.

2.2. *The ray curvature*

In differential geometry, the curvature κ is defined as the change in the tangent vector $\boldsymbol{t}$, along the arc length

$$\kappa \boldsymbol{n} = \frac{\mathrm{d}\boldsymbol{t}}{\mathrm{d}s}, \tag{2.10}$$

where $\boldsymbol{n}$ is the ray normal vector, and thus the identity $\boldsymbol{t} \perp \boldsymbol{n}$ is admitted such that $\boldsymbol{n} = [-t_y, t_x]$ is defined. The expression (2.7*b*) can therefore be re-written in a form as follows:

$$\dot{\boldsymbol{r}} = \dot{s}\boldsymbol{t}. \tag{2.11}$$

On the insertion of (2.10) into (2.11), the curvature κ, of rays can be expressed in a parametric form as follows (e.g. Mathiesen 1987):

$$\kappa = \frac{\dot{x}_r \ddot{y}_r - \dot{y}_r \ddot{x}_r}{\left[(\dot{x}_r)^2 + (\dot{y}_r)^2\right]^{3/2}} \equiv \boldsymbol{t} \cdot \frac{[\ddot{y}_r, -\ddot{x}_r]}{(\dot{x}_r)^2 + (\dot{y}_r)^2}, \tag{2.12}$$

where the double dots denotes the second-order derivative with respect to time. Here, we opted for the signed version of the curvature, in order to be compliant with previous works (e.g. Kenyon 1971; Gallet & Young 2014; Bôas & Young 2020). It is now clearly seen in (2.12) that the curvature relies on an explicit expression for both the unit tangent vector of the rays and the second derivative of the ray trajectories with respect to time. The latter can be obtained by definition

$$\frac{\mathrm{d}^2\boldsymbol{r}}{\mathrm{d}t^2} = [\ddot{x}_r, \ddot{y}_r] \text{ or } \frac{\mathrm{d}^2\boldsymbol{r}}{\mathrm{d}t^2} = \frac{\mathrm{d}}{\mathrm{d}t}(\boldsymbol{U} + \boldsymbol{c}_g), \tag{2.13a,b}$$

the latter of which should be evaluated on the time-dependent rays, i.e. $\boldsymbol{x} = \boldsymbol{r}(t)$ should be noted for (2.13*b*). Thereby, we arrive at

$$\frac{\mathrm{d}^2\boldsymbol{r}}{\mathrm{d}t^2} = \partial_t \boldsymbol{U} + \left(\frac{\mathrm{d}\boldsymbol{x}}{\mathrm{d}t} \cdot \nabla\right)\boldsymbol{U} + \left(\frac{\mathrm{d}\boldsymbol{x}}{\mathrm{d}t} \cdot \nabla\right)\boldsymbol{c}_g(\boldsymbol{k}, \boldsymbol{x}) + \left(\frac{\mathrm{d}\boldsymbol{k}}{\mathrm{d}t} \cdot \nabla_k\right)\boldsymbol{c}_g(\boldsymbol{k}, \boldsymbol{x}), \tag{2.14}$$

for $\boldsymbol{x} = \boldsymbol{r}(t)$, where $\mathrm{d}/\mathrm{d}t$ denotes the material derivative with respective to time. Expression (2.14) can be simplified by applying the quasi-stationary background current assumption $\partial_t \boldsymbol{U} \simeq \boldsymbol{0}$, meaning that the background current $\boldsymbol{U}$ is slowly varying in time compared with the rapidly varying phase and rays. The terms on the right-hand side of (2.14) can be otherwise readily evaluated by also applying (2.6*b*).

Inserting (2.4*a*,*b*), (2.9), (2.14) and (2.6*b*) into (2.12) and keeping the terms to $\mathcal{O}(\varepsilon)$ eventually gives rise to the explicit expression of the ray curvature as follows:

$$\kappa_{\approx} = \frac{\partial_x U_2 - \partial_y U_1}{c_g} + \frac{\boldsymbol{e}_{k,\perp} \cdot \boldsymbol{\nabla} c}{c_g}. \tag{2.15}$$

Here, the assumption of $\partial_t \boldsymbol{U} \simeq \boldsymbol{0}$ was used, and the subscript '$\approx$' denotes an approximation to the curvature according to (2.12). We recall that the local curvature of the rays given by (2.15) was derived under the weak current and geometric optics approximations; the unit vector $\boldsymbol{e}_{k,\perp} = [-k_y, k_x]/k$ was defined, which obeys $\boldsymbol{e}_k \cdot \boldsymbol{e}_{k,\perp} = 0$, suggesting that it is always orthogonal to the local wave vectors. We remark that the identities $\boldsymbol{\nabla} c = \boldsymbol{\nabla} h \partial_h c$ and $c(k, \boldsymbol{x}) = \sqrt{g \tanh kh(\boldsymbol{x})/k}$ are admitted in (2.15) where the terms are all evaluated on the time-dependent rays: $\boldsymbol{x} = \boldsymbol{r}(t)$.

For deep water waves which admit $\boldsymbol{\nabla} c = \boldsymbol{0}$, the local curvature of the rays by (2.15) recovers the expressions by Kenyon (1971) and Dysthe (2001) and, for the cases in the absence of current, it recovers Arthur *et al.* (1952, their expression (1*c*)). We also note that the current-gradient term in (2.15) can be expressed by the vertical component of the vorticity vector $\zeta = \partial_x U_2 - \partial_y U_1$.

It shall be noted that the approximate curvature (2.15) can also be recovered from the exact form by Phillips (1977, their (3.5.6)) using the same assumptions associated with the current and bathymetry. Compared with this exact but more complex form, the leading-order approximation $\kappa_{\approx}$ enables a direct evaluation of the individual effects of current- or bathymetry-gradient on the wave refraction.

3. Limiting cases for wave refraction

In this section, we examine effects of both current and bathymetry on the wave refraction using a few limiting cases. To this end, we firstly assess the accuracy in the analytical approximation given by (2.15) by direct numerical simulations presented in § 3.1 and next elucidate the underlying novel physics using a few example cases presented in § 3.2. For the ray path predictions essential for the results presented in this section, we use the open-source ray tracing solver developed by Halsne *et al.* (2023).

3.1. *Model validation*

To validate the approximate curvature $\kappa_{\approx}$ denoted by (2.15), we compare its numerical predictions with those based on the direct numerical implementation of the definition according to (2.12). With the ray paths, the curvature based on (2.15) can be directly evaluated on the wave rays $\boldsymbol{x} = \boldsymbol{r}(t)$ for the time instants $t = n\Delta t$ with $n \in [0, 1, 2, \ldots, N_t - 1]$, where Δt and N_t denote the time interval and total number of time steps used for the numerical results, and $T = \Delta t (N_t - 1)$. Similarly, the curvature based on (2.12) was readily evaluated applying a second-order accurate central difference scheme on $\boldsymbol{r}(t)$.

We follow Kenyon (1971) as analytical solutions exist for both the ray paths and the material derivative of the wave vector expressed as (2.4) and (2.6), respectively (Longuet-Higgins & Stewart 1961). In particular, we consider a deep water wave train on a constant

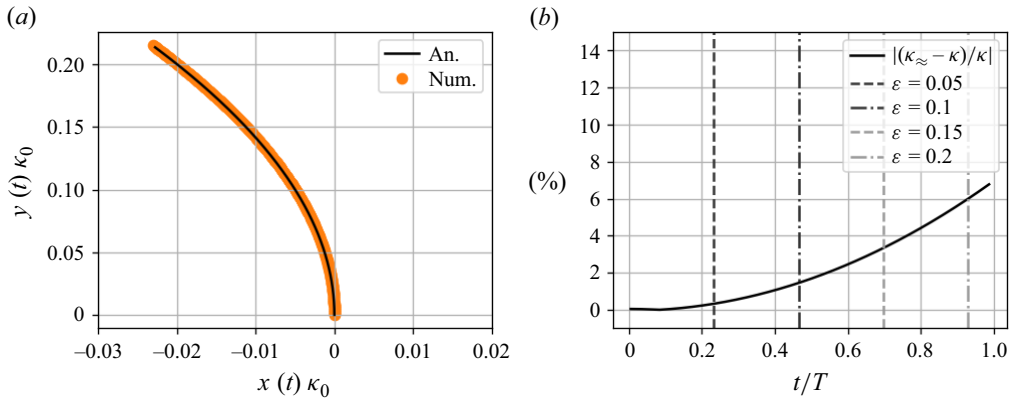

Figure 1. Accuracy in (2.15) for a deep water 6 s period wave on a shearing current starting at point $\boldsymbol{x}_r(0) = (0, 0)$. Panel (*a*) show the analytical ray path (black solid line) and modelled (orange dots) from numerical integration of the ray equations (2.4) and (2.6). The ray paths are normalised with the initial curvature κ_0. Indeed, the shape of the normalised ray paths are independent of the shear magnitude and wave period. Panel (*b*) demonstrates the temporal evolution in percentage difference between κ and $\kappa_{\approx}$ for the ray in panel (*a*). Vertical lines denote different values of $\varepsilon = U_1(y)/c_g$.

shear current

$$\boldsymbol{U} = [\tau y, 0], \tag{3.1}$$

for $y > 0$, where τ is the velocity shear. Inserting the current profile described by (3.1) into the approximate curvature leads to $\kappa_{\approx} = |\tau/c_g|$, where it has been shown by Kenyon (1971) that this approximation leads to a difference with (2.12) by approximately 10 % for $\varepsilon \sim 0.05$.

The finding reported by Kenyon (1971) is consistent with the comparison shown in figure 1. Here, the temporal evolution of wave rays with initial position $\boldsymbol{x}_r(0) = (0, 0)$ and initial propagation direction $\theta_0 = \pi/2$ were used, where $\boldsymbol{e}_k \perp \boldsymbol{u}$ is implied. Here, and throughout the text, subscript '0' refers to initial conditions, i.e. $t = 0$. Such rays admit the analytical form $x_r(t) = -y_r(t)^2\kappa_0/2$ (Kenyon 1971), where $\kappa_0 = -2\tau\Omega_0/\mathrm{g}$ denotes the initial curvature, and Ω_0 the initial intrinsic frequency. Here, the initial frequency corresponded to a 6 s period wave. Figure 1(*a*) demonstrates a good agreement between the ray path predictions by the ray tracing solver and the analytical approximation. As expected, the relative difference between $\kappa_{\approx}$ and κ, being defined as $|(\kappa_{\approx} - \kappa)/\kappa|$, grows in time due to the constant shear τ and the increase in current speed with y (figure 1*b*); it reaches approximately 6 % for $\varepsilon = 0.2$, which well falls within the regime as reported by Kenyon (1971).

3.2. *Wave refraction by both current and bathymetry*

Our derivations in § 2 have demonstrated that the presence of both current and a varying bathymetry can lead to complex interplay, and thereby play an important role in wave refraction. Roles due to current and a bathymetry can in particular be quantified in a separate manner by noting that the approximate curvature $\kappa_{\approx}$ expressed as (2.15) has the form of linear superposition of current- and bathymetry-altered curvature components denoted by κ_c and κ_d, respectively, where

$$\kappa_c = \frac{\partial_x U_2 - \partial_y U_1}{c_g} \quad \text{and} \quad \kappa_d = \frac{\boldsymbol{e}_{k,\perp} \cdot \boldsymbol{\nabla} c}{c_g} \text{ such that } \kappa_{\approx} = \kappa_c + \kappa_d. \tag{3.2a,b,c}$$

Abbreviation	f_0 (Hz)	H (m)	α	U_* (m s^{-1})	k_0h_0	L_x (km)	L_y (km)
VD	0.08	150	0.95	—	2	20	10
DW	0.08	10,000	0	—	$\gg \pi$	20	10
PC	0.08	—	—	0.6	2	20	10
NC	0.08	—	—	−0.6	2	20	10

Table 1. Values for the ambient conditions including VDs, DW, PC and NC current profiles used in the numerical ray tracing simulations in figures 2–4. Subscript '0' refers to initial conditions.

Here, (3.2*c*) permits us to quantify the individual and combined contributions of current and depth to the wave refraction, as noted, where both the sign and magnitude of κ_c and κ_d determine the ultimate effect on the wave refraction. We will use a few limiting cases in the following subsections to explicitly explore the underlying physics. These cases include wave trapping – corresponding to a wave ray which cannot escape – and zero curvature when $\kappa_c = -\kappa_d$. In particular, the wave trapping is typically manifested as total internal reflection, like waves on an opposing current jet or atop an elongated submarine shallow, or as a complete absorption, like waves propagating against a beach.

3.2.1. *Wave trapping on jet-like currents and complex bathymetry*

To demonstrate the wave trapping phenomena due to the joint influence of current and depth on the wave refraction, we use the bathymetry profile and jet-like current, being expressed as, respectively,

$$h(x,\,y) = \frac{H}{2}\left(1+\alpha\,\sin\left(\pi\,\frac{x}{L_x}\right)\cos\left(\pi\,\frac{y}{L_y}\right)\right) \quad \text{and} \quad \boldsymbol{U} = \left[U_*\cos^4\left(\pi\,\frac{y}{L_y}-\frac{\pi}{2}\right),\,0\right]. \tag{3.3a,b}$$

Here, L_x and L_y are the characteristic length in the x- and y-directions, respectively; H denotes the characteristic length in the depth direction; $\alpha \in [0,\,1]$ denotes the degree of varying bathymetry, leading to the measure of the bathymetry variation in the x- and y-directions being $\max|\nabla h/h|$. When $\mathcal{O}(\max|\nabla h/h|/k) \ll 1$ it corresponds to a slowly varying bathymetry in the horizontal plane, as required in the assumption for the approximate curvature $\kappa_{\approx}$. Likewise, U_* denotes a characteristic current magnitude in the x-direction. The corresponding slowly varying current assumption is fulfilled for $\mathcal{O}(\max|\nabla \boldsymbol{U}/U|/k) \ll 1$, where $U = |\boldsymbol{U}|$ (Peregrine 1976). Here, and for the subsequent analysis, $L_x = 20$ km, $L_y = 10$ km and a wave period of 12 s has been used, unless otherwise stated. The remaining parameters chosen for the numerical predictions are listed in table 1.

Figure 2 shows the role of depth-induced refraction on wave propagation, using a variable depth (VD) obtained by (3.3*a*) by letting $\alpha = 0.95$. For this profile, $h \in [3.75,\,146.25]$ m and the shallowest region simulates a seamount. As expected, waves are refracted according to the water-depth gradients, and thus bend towards the shallower regions. The seamount attracts and traps a large portion of the wave rays which are initially located at $y > 0.5L_y$. The bathymetry-altered curvature κ_d obtains its largest magnitude for the rays located in the vicinity of the local seamount, but having slightly passed it (see figure 2*b* around $(0.6L_x,\,0.8L_y)$).

Refraction solely due to currents are shown by simulations in DW conditions, which include a positively (PC) and negatively oriented current jet (NC). The PC induces caustics at the edges of the jet, while the NC induces caustics at the centre of the jet (figure 3*a*,*b*).

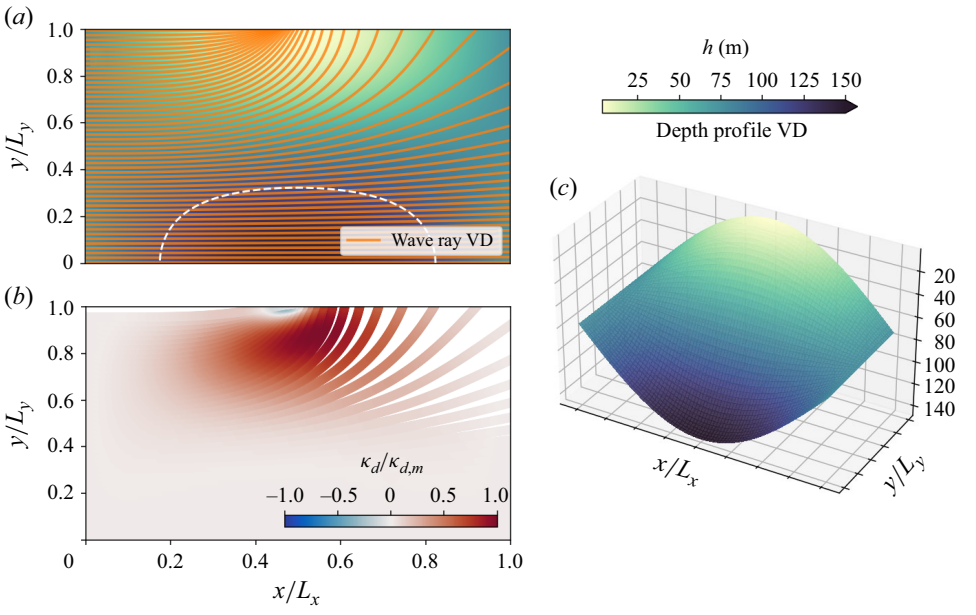

Figure 2. The influence by the variable depth (VD table 1) on the wave propagation. Panel (*a*) show a wave ray with initial period of 12 s propagating from left to right, with initial propagation direction parallel to the x-axis. The bathymetry-altered curvature κ_d, normalised by its maximum value $\kappa_{d,m} = \max|\kappa_d|$, is shown in panel (*b*). The shallowest region in the VD bathymetry simulates a seamount and is shown in panel (*c*), where the water depth h is given by the background colour. White dashed line in panel a denote the $h = \lambda/2$ contour.

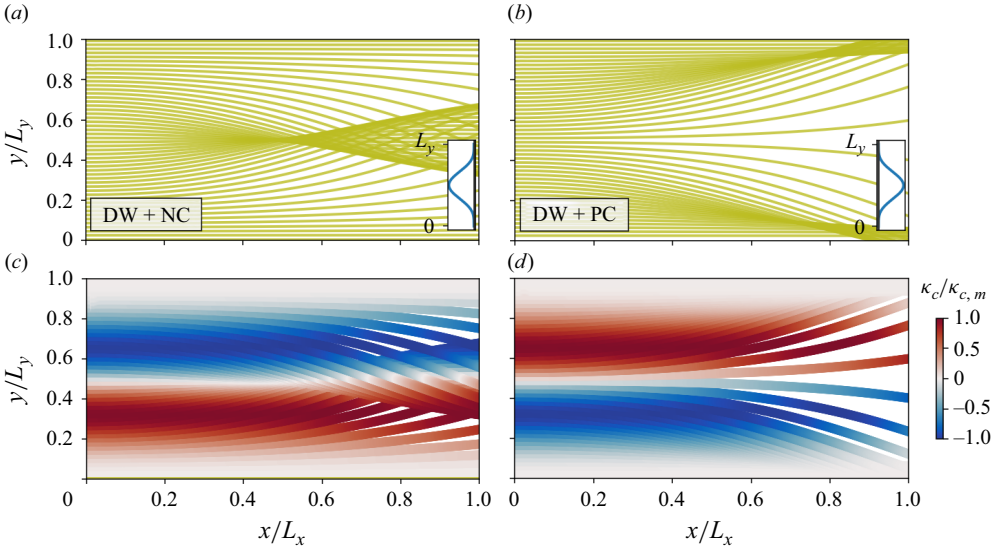

Figure 3. Refraction of deep water (DW) 12 s period waves atop a negatively (NC) and positively oriented current (PC) are shown in panels (*a*) and (*b*), respectively. The waves initially propagate from left to right. Inset figures denote the current profiles and their orientation, with further details given in table 1. Panels (*c*) and (*d*) show the associated current-altered curvature κ_c along each wave ray, which is normalised by its maximum value $\kappa_{c,m} = \max|\kappa_c|$.

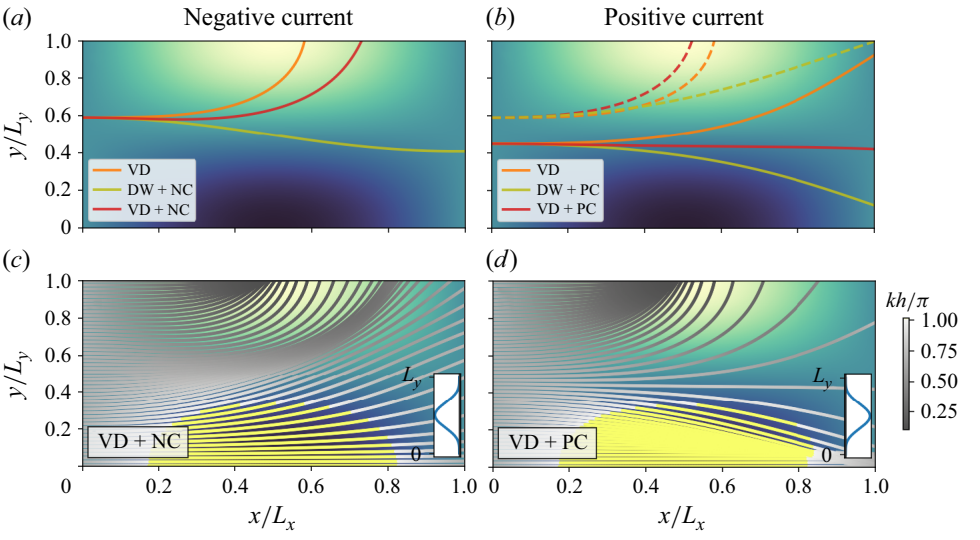

Figure 4. The joint influence by VD and jet-like currents (NC, PC) on wave propagation. Initial wave periods are 12 s. Upper panels show the difference in propagation between depth-only (VD, orange), current-only (yellow) and their joint influence (red), when starting at the same initial position; dashed and solid lines in panel *b* denote different initial positions. Lower panels show the refraction for several wave rays on the negative current (panel *c*) and positive current (panel *d*). The colour shading denote kh/π, where yellow colour denote $kh/\pi \geqslant 1$.

If the domain for the NC case were extended in the x-direction, we would have seen the characteristic wave trapping phenomenon at the centre of the jet (Peregrine 1976). In this example, the current-induced curvature κ_c is given by

$$\kappa_c = \frac{-2U_*\pi}{L_y c_g} \cos^2\left(\pi \frac{y}{L_y} - \frac{\pi}{2}\right) \sin\left(\pi \frac{2y}{L_y} - \pi\right). \tag{3.4}$$

Here, the sign of κ_c is mirrored about the line $y = 0.5L_y$ for the two cases (figure 3*c*,*d*).

The joint influence by the bathymetry and current yield more complicated situations (figure 4). Combining the varying depth and negative current (VD + NC) causes two caustics; one is located at the local shallow and the other takes the form of a meandering tube steered by the bathymetry (figure 4*c*). Conversely, when the current is positive, there is a stronger refraction against the local shallow since the following current and bathymetry work together (VD + PC, figure 4*d*); this leads to a corresponding decrease of wave rays in the region where $x > 0.5L_X$ and $y > 0.5L_y$, when compared with the VD-only case (see figure 2*a*). However, when combining the variable currents and bathymetry, we do recognise the predominant wave ray propagation patterns from the isolated cases; the refraction against the local shallow (figure 2*a*); the caustic at the centre of the opposing jet (figure 3*a*); and the diverging wave ray pattern at the centre of the following jet (figure 3*b*).

The combined depth- and current-induced refraction is further highlighted by comparing the ray paths in different cases. Figure 4(*a*,*b*) shows the ray paths which initiate at the same position of $(0, 0.6L_y)$ but are affected by either the PC, NC, VD or the combined effects of a current and VD. We see that the effect by the NC is to extend the distance where the ray holds a substantial k_x component compared with the VD solution. As a consequence, the wave ray exits the domain further away from the local shallow, which is illustrated by the red line of figure 4(*a*). The opposite is true for the PC case,

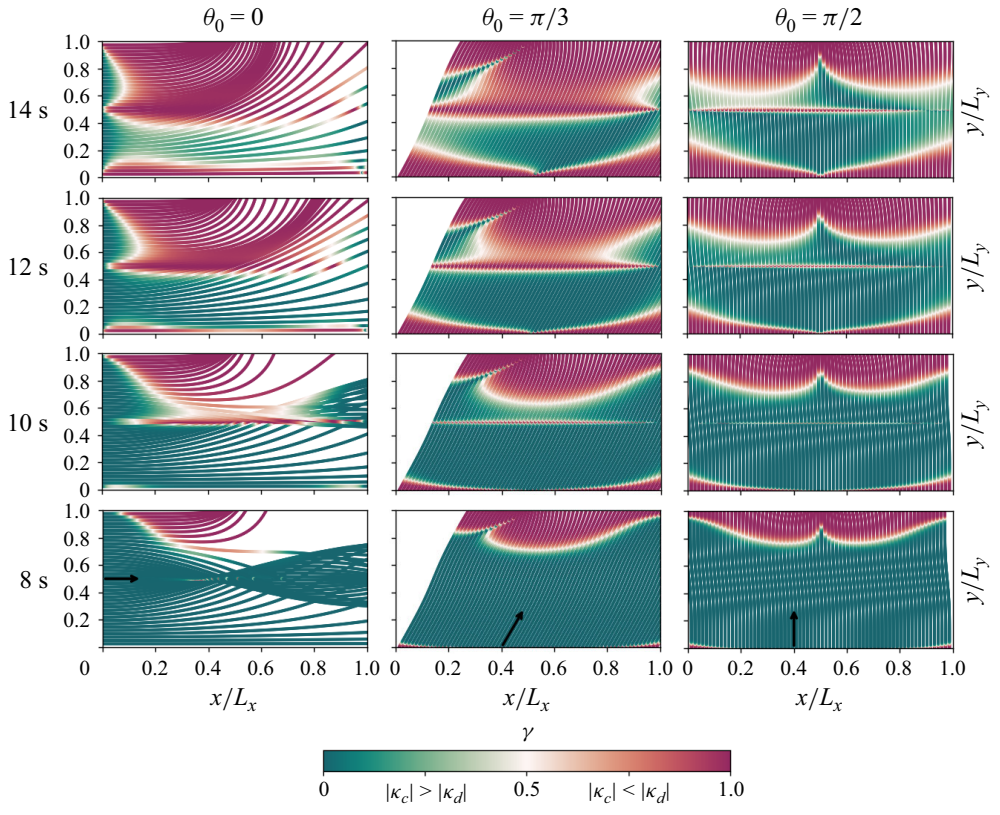

Figure 5. The ray curvature ratio γ computed locally along wave rays. Rows from top to bottom show ray tracing simulations for waves with initial periods of 14, 12, 10 and 8 s, respectively. Columns from left to right denote different initial propagation directions θ_0, as indicated by the arrows in the lower row plots. All model simulations have the conditions VD + NC (table 1).

where the current gradients refract the wave ray against the VD faster than the bathymetry alone, as is shown by the red dashed line in figure 4(*b*). Thus, the joint effect of the PC and VD is stronger than their individual contribution.

We also depict in figure 4(*b*) the rays with an initial position of $(0, 0.44L_y)$. Here, the gradients of the positive current PC almost resemble the gradient of VD, but with different signs, leading to a wave ray with a small curvature, as is illustrated by the solid red line in figure 4(*b*). Such a case will be investigated in more detail in the subsequent subsection.

We introduce the ratio

$$\gamma = \kappa_d^2/\left(\kappa_d^2 + \kappa_c^2\right), \tag{3.5}$$

such that $\gamma \in [0, 1]$, which is referred to as the refraction assessment metric because, particularly when κ_c and κ_d hold the same sign, it can be used to measure which of the two plays a more dominant role in the wave refraction. Specifically, κ_d and κ_c dominates for $\gamma > 0.5$ and $\gamma < 0.5$, respectively.

The metric (3.5) is shown in figure 5 for an ensemble of ray tracing simulations, including four different initial wave periods and three initial directions, while propagating atop VD + NC. Besides mapping when and where depth- and current-induced refractions dominate, the results highlight some important physical aspects concerning the two refraction mechanisms. Firstly, figure 5 demonstrates that the horizontal extent of the

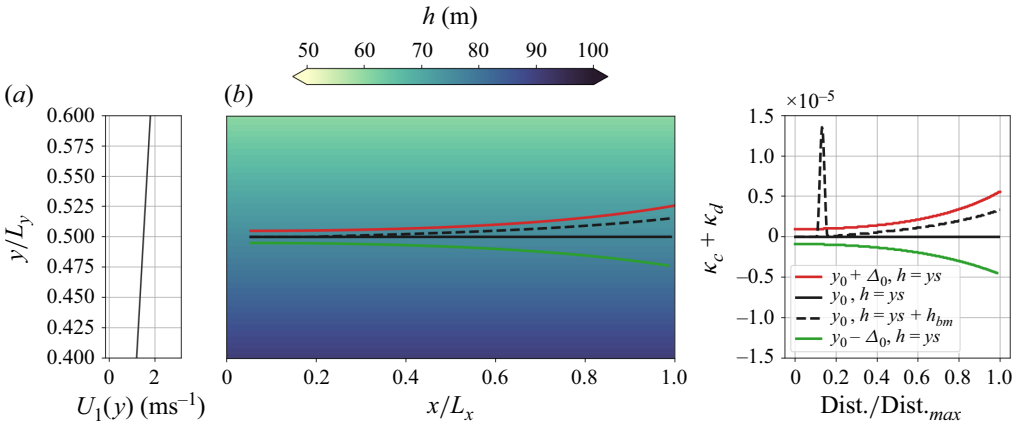

Figure 6. A special case where depth and current refraction equalise and cancel each other. Panel (*b*) show wave rays propagating from left to right atop a sloping beach in the y-direction and a shear current of type (3.1) (see panel (*a*). The black solid ray, where $\kappa_c = -\kappa_d$, is initially located at $\boldsymbol{x}_r(0) = (0.05L_x, y_0)$, where $y_0 = 0.5L_y$. Adjacent rays are perturbed $\pm\Delta_0 = \pm 0.005L_y$ in the y-direction. Panel (*c*) show the evolution of $\kappa_c + \kappa_d$ along the wave propagation distance (Dist.). Dashed black line denotes a slightly modified twin experiment which adds a small bump in the bathymetry ($h = ys + h_{bm}$) in a subset of the domain, with details outlined in the text.

bathymetry dominated refraction κ_d increases with increasing wave period. This relation is due to the two following reasons: (i) kh increases with wave period meaning that longer waves feel more the depth change than shorter ones (Kenyon 1983), and thus scatter accordingly; (ii) both terms in $\kappa_{\approx}$ are inversely proportional to the group velocity c_g, meaning that decreasing wave periods strengthen the contribution from κ_c. Secondly, figure 5 highlights the directional dependence of κ_d; the regions dominated by depth refraction (redish colours) have a different horizontal extent when comparing the leftmost and rightmost columns in figure 5. The reason for this difference is that the depth gradients $\partial_x h \neq \partial_y h$, and that the unit vector $\boldsymbol{e}_{k,\perp} = [-k_y, k_x]/k$ generally holds different values depending on the initial direction. As a consequence, κ_d obtains different values. On the contrary, and as seen from (3.4), κ_c does not have such directional dependence.

3.2.2. *Zero curvature*

As highlighted in figure 4(*b*), zero curvature occurs when κ_c and κ_d have different signs but with a similar magnitude, i.e. $\kappa_c = -\kappa_d$. Such situations thus prevent wave refraction. This is illustrated in figure 6 for a prescribed shear current described by (3.1) with $\tau = 0.0015\ \mathrm{s}^{-1}$ and a constant sloping beach in the y-direction. Here, the depth

$$h(x, y) = ys, \tag{3.6}$$

where $s = 0.015$. This example can be used to represent the circumstances where oblique waves enter a gently sloping beach which is subject to longshore currents. To construct a wave ray which recovers $\kappa_c = -\kappa_d$ in the x-direction, we solve the implicit equation for wavenumber k

$$\nabla c = \frac{1}{2}\sqrt{\frac{gk}{\tanh(kh)}}\left[1 - \tanh^2(kh)\right]\nabla h. \tag{3.7}$$

We consider the initial position $\boldsymbol{x}_r(0) = (0.05L_x, y_0)$, where $y_0 = 0.5L_y$ and the water depth $h = 75$ m. Then, (3.7) yields a wave period of 12.7 s, and $kh = 1.95$. The resulting

wave ray becomes a straight line when the initial propagating direction is parallel to the x-axis, and the wave propagates from left to right (figure 6*b*). However, small changes in the initial position are decisive for the ray direction. We introduce the small perturbation in position $\Delta_0 = 0.005L_y$, which corresponds to 50 m. The wave ray becomes trapped by the bathymetry if initially located at $y_0 + \Delta_0$, i.e. 50 m closer to shore (red line figure 6). On the contrary, the ray escapes the bathymetry if initially located Δ_0 further away from shore ($y_0 - \Delta_0$, green line).

In cases with zero refraction, the wave refraction is very sensitive to any modulation in wavenumber. This is illustrated in a slightly modified twin experiment where the sloping beach is subject to a small perturbation, in the form of a small bump in the bathymetry. Let

$$h_{bm} = 10 \sin\left(\frac{\pi}{0.05L_x}(x - 0.15L_x)\right) \cos\left(\frac{\pi}{0.1L_y}(0.5 + y - 0.45L_y)\right), \tag{3.8}$$

represent a local shallow bank, such that $h = ys + h_{bm}$ in the region $x \in [0.15L_x, 0.2L_x]$ and $y \in [0.45L_y, 0.55L_y]$. Such a model realisation is depiced by the dashed lines in figure 6(*b*,*c*); while k starts to decrease on the hump, ∇c starts increasing such that κ_c starts dominating. Indeed, the effect of the hump is that the wave ray eventually gets trapped by the bathymetry.

4. Conclusions

In this paper, we have examined the complex effects of varying current and depth on the refraction of surface gravity waves. The study is carried out through a newly derived analytical approximation to the wave ray curvature described by (2.15) under the assumption of weak current and slowly varying bathymetry. Particularly, the current is assumed to propagate in the same plane as the wave vector, has a depth-uniform velocity profile and varies slowly in time compared with the phase of the characteristic waves. The approximate curvature recovers to Arthur *et al.* (1952), Kenyon (1971) and Dysthe (2001) for the cases in deep water and the absence of current, respectively, and has a less complex form than the exact solution by Phillips (1977, § 3.5). It is also validated by the open-source ray tracing framework developed by Halsne *et al.* (2023).

The explicit expression of the approximate curvature (2.15) is in the form of linear superposition of a current- (κ_c) and depth-gradient-induced component (κ_d), allowing us to quantify the individual and combined contributions of current and depth to the wave refraction. It indicates that both the sign and magnitude of κ_c and κ_d play important roles in wave refraction, which have been explicitly explored in a few limiting cases. When κ_c and κ_d hold the same and opposite sign, the current- and depth-induced components together lead to an enhanced and reduced effect on wave refraction, respectively, compared with their individual contributions. Which of the two plays the dominant role depends on the relative magnitudes of κ_c and κ_d. When $\kappa_c\kappa_d > 0$, the refraction assessment metric γ ($\gamma \in [0, 1]$) described by (3.5) is proposed. For the special cases where $\kappa_c + \kappa_d \approx 0$, we address the fact that additional perturbations due to either a current- or depth-induced gradient, even with a small magnitude, can lead to noticeable deviation of the wave propagation direction from its original path in a long distance.

We note that the current and bathymetry can influence each other, contributing to complex physics such as additionally induced waves and modified surface elevation (see e.g. Buttle *et al.* 2018; Akselsen & Ellingsen 2019). Albeit some of these effects are represented in e.g. ocean circulation models, ray tracing simulations are also expected to account for any change in the ambient media, such as the variant vertical bathymetry datum

induced by severe storm surge. The interdependence between current and bathymetry beyond the applicability regime of the derived model will be addressed in future works.

The results reported here rely on a theoretical model with explicitly stated assumptions. In other words, the model is limited in its applicability. For instance, it cannot be used to deal with currents whose velocity gradient in the horizontal plane is strong (Shrira & Slunyaev 2014), currents whose velocity profile is depth-dependent (Stewart & Joy 1974; Kirby & Chen 1989; Ellingsen & Li 2017; Quinn, Toledo & Shrira 2017; Li & Ellingsen 2019) or water regions of a sudden depth change (Trulsen *et al.* 2020; Li & Chabchoub 2023). Nevertheless, the results from this paper are expected to hold for most practical circumstances in coastal waters and can be readily used in developing new post-processing approaches essential to remote sensing, such as the recovery of current profiles and bathymetry through the measurement of surface waves (see, e.g. Smeltzer *et al.* 2019). Future works will consider the impact by depth and current refraction on the wave intensity modulation, and thus possibly extend the works by Munk & Arthur (1952) and Jonsson & Wang (1980).

Acknowledgements. We thank the anonymous reviewers for their suggestions which have significantly improved the quality of the manuscript. T.H. would like to thank Dr K.H. Christensen and Dr MP. Malila for fruitful discussions throughout this work. T.H. acknowledges the financial support from the Norwegian Space Agency through the *CoastCurr* project (Nb. 74CO2501).

Funding. Y. L. acknowledges the financial support from an European Research Council (ERC) - Starting grant (*OceanCoupling*, grant agreement ID: 101164343). Views and opinions expressed are, however, those of the authors only and do not necessarily reflect those of the European Union or the ERC Executive Agency. Neither the European Union nor the granting authority can be held responsible for them.

Declaration of interests. The authors report no conflict of interest.

References

Akselsen, A.H. & Ellingsen, S.Å. 2019 Sheared free-surface flow over three-dimensional obstructions of finite amplitude. *J. Fluid Mech.* **878**, 740–767.

Ardhuin, F., Gille, S.T., Menemenlis, D., Rocha, C.B., Rascle, N., Chapron, B., Gula, J. & Molemaker, J. 2017 Small-scale open ocean currents have large effects on wind wave heights. *J. Geophys. Res. Oceans* **122** (6), 4500–4517.

Arthur, R.S. 1950 Refraction of shallow water waves: the combined effect of currents and underwater topography. *EOS Trans. Am. Geophys. Union* **31** (4), 549–552.

Arthur, R.S., Munk, W. & Isaacs, J.D. 1952 The direct construction of wave rays. *EOS Trans. Am. Geophys. Union* **33** (6), 855–865.

Bôas, A.B.V., Cornuelle, B.D., Mazloff, M.R., Gille, S.T. & Ardhuin, F. 2020 Wave–current interactions at meso-and submesoscales: insights from idealized numerical simulations. *J. Phys. Oceanogr.* **50** (12), 3483–3500.

Buttle, N.R., Pethiyagoda, R., Moroney, T.J. & McCue, S.W. 2018 Three-dimensional free-surface flow over arbitrary bottom topography. *J. Fluid Mech.* **846**, 166–189.

Bôas, A.B.V. & Young, W.R. 2020 Directional diffusion of surface gravity wave action by ocean macroturbulence. *J. Fluid Mech.* **890**, R3-1–R3-12.

Dysthe, K.B. 2001 Refraction of gravity waves by weak current gradients. *J. Fluid Mech.* **442**, 157–159.

Ellingsen, S.Å. & Li, Y. 2017 Approximate dispersion relations for waves on arbitrary shear flows. *J. Geophys. Res. Oceans* **122** (12), 9889–9905.

Gallet, B. & Young, W.R. 2014 Refraction of swell by surface currents. *J. Mar. Res.* **72** (2), 105–126.

Halsne, T., Bohlinger, P., Christensen, K.H., Carrasco, A. & Breivik, Ø. 2022 Resolving regions known for intense wave–current interaction using spectral wave models: a case study in the energetic flow fields of Northern Norway. *Ocean Model.* **176**, 102071.

Halsne, T., Christensen, K.H., Hope, G. & Breivik, Ø. 2023 Ocean wave tracing v.1: a numerical solver of the wave ray equations for ocean waves on variable currents at arbitrary depths. *Geosci. Model Dev.* **16** (22), 6515–6530.

HESSNER, K., REICHERT, K., BORGE, J.C.N., STEVENS, C.L. & SMITH, M.J. 2014 High-resolution X-Band radar measurements of currents, bathymetry and sea state in highly inhomogeneous coastal areas. *Ocean Dyn.* **64**, 989–998.

HJELMERVIK, K. & TRULSEN, K. 2009 Freak wave statistics on collinear currents. *J. Fluid Mech.* **637**, 267–284.

JONSSON, I.G. & WANG, J.D. 1980 Current-depth refraction of water waves. *Ocean Engng* **7** (1), 153–171.

KENYON, K.E. 1971 Wave refraction in ocean currents. *Deep-Sea Res. Oceanogr. Abstracts* **18** (10), 1023–1034.

KENYON, K.E. 1983 On the depth of wave influence. *J. Phys. Oceanogr.* **13** (10), 1968–1970.

KIRBY, J.T. & CHEN, T.-M. 1989 Surface waves on vertically sheared flows: approximate dispersion relations. *J. Geophys. Res. Oceans* **94**, 1013–1027.

KLOTZ, A.N., ALMAR, R., QUENET, Y., BERGSMA, E.W.J., YOUSSEFI, D., ARTIGUES, S., RASCLE, N., SY, B.A. & NDOUR, A. 2024 Nearshore satellite-derived bathymetry from a single-pass satellite video: Improvements from adaptive correlation window size and modulation transfer function. *Remote Sens. Environ.* **315**, 114411.

LANDAU, L.D. & LIFSHITZ, E.M. 1987 *Fluid Mechanics*. 2nd edn, vol. 6. Pergamon Press.

LAVRENOV, I.V. 2003 *Wind-Waves in Oceans: Dynamics and Numerical Simulations*. 2nd edn. Springer.

LENAIN, L., SMELTZER, B.K., PIZZO, N., FREILICH, M., COLOSI, L., ELLINGSEN, S.Å., GRARE, L., PEYRIERE, H. & STATOM, N. 2023 Airborne remote sensing of upper-ocean and surface properties, currents and their gradients from meso to submesoscales. *Geophys. Res. Lett.* **50** (8), 1–11.

LI, Y. & CHABCHOUB, A. 2023 On the formation of coastal rogue waves in water of variable depth. *Camb. Prisms: Coast. Futures* **1**, e33.

LI, Y. & ELLINGSEN, S.Å. 2019 A framework for modeling linear surface waves on shear currents in slowly varying waters. *J. Geophys. Res.: Oceans* **124** (4), 2527–2545.

LONGUET-HIGGINS, M.S. & STEWART, R.W. 1961 The changes in amplitude of short gravity waves on steady non-uniform currents. *J. Fluid Mech.* **10** (4), 529–549.

LUND, B., GRABER, H.C., TAMURA, H., C.O. COLLINSIII & VARLAMOV, S.M. 2015 A new technique for the retrieval of near-surface vertical current shear from marine x-band radar images. *J. Geophys. Res.: Oceans* **120** (12), 8466–8486.

MATHIESEN, M. 1987 Wave refraction by a current whirl. *J. Geophys. Res. Oceans* **92** (C4), 3905–3912.

MEI, C.C., STIASSNIE, M. & YUE, D.K.P. 2005 *Theory and Applications of Ocean Surface Waves. Part 1: Linear Aspects*. Advanced Series on Ocean Engineering, vol. 23. World Scientific.

MUNK, W.H. & ARTHUR, R.S. 1952 Wave intensity along a refracted ray. In *Proceedings of NBS Semicentennial Symposium on Gravity Waves Held at the NBS on June 18-20 1951*, vol. 521, pp. 95. NBS.

ONORATO, M., PROMENT, D. & TOFFOLI, A. 2011 Triggering rogue waves in opposing currents. *Phys. Rev. Lett.* **107** (18), 184502.

PEREGRINE, D.H. 1976 Interaction of water waves and currents. In *Advances in Applied Mechanics*, (ed. Chia-Shun Yih), vol. 16, pp. 9–117. Elsevier.

PHILLIPS, O.M. 1977 *The Dynamics of the Upper Ocean*, 2nd edn. Cambridge University Press.

QUILFEN, Y., YUROVSKAYA, M., CHAPRON, B. & ARDHUIN, F. 2018 Storm waves focusing and steepening in the Agulhas current: satellite observations and modeling. *Remote Sens. Environ.* **216**, 561–571.

QUINN, B.E., TOLEDO, Y. & SHRIRA, V.I. 2017 Explicit wave action conservation for water waves on vertically sheared flows. *Ocean Model.* **112**, 33–47.

ROMERO, L., HYPOLITE, D. & MCWILLIAMS, J.C. 2020 Submesoscale current effects on surface waves. *Ocean Model.* **153**, 101662.

SHRIRA, V.I. & SLUNYAEV, A.V. 2014 Nonlinear dynamics of trapped waves on jet currents and rogue waves. *Phys. Rev. E* **89** (4), 041002.

SMELTZER, B.K., ÆSØY, E., ÅDNØY, A. & ELLINGSEN, S.Å. 2019 An improved method for determining near-surface currents from wave dispersion measurements. *J. Geophys. Res.: Oceans* **124** (12), 8832–8851.

SMIT, P.B. & JANSSEN, T.T. 2019 Swell propagation through submesoscale turbulence. *J. Phys. Oceanogr.* **49** (10), 2615–2630.

SMITH, R. 1976 Giant waves. *J. Fluid Mech.* **77** (3), 417–431.

STEWART, R.H. & JOY, J.W. 1974 HF radio measurements of surface currents. *Deep-Sea Res.* **21** (12), 1039–1049.

TRULSEN, K., RAUSTØL, A., JORDE, S. & RYE, L.B. 2020 Extreme wave statistics of long-crested irregular waves over a shoal. *J. Fluid Mech.* **882**, R2.

WANG, H., BÔAS, A.B.V., YOUNG, W.R. & VANNESTE, J. 2023 Scattering of swell by currents. *J. Fluid Mech.* **975**, A1.

WHITE, B.S. & FORNBERG, B. 1998 On the chance of freak waves at sea. *J. Fluid Mech.* **355**, 113–138.

WHITHAM, G.B. 1965 A general approach to linear and non-linear dispersive waves using a Lagrangian. *J. Fluid Mech.* **22** (2), 273–283.

ZHENG, Z., LI, Y. & ELLINGSEN, S.Å. 2023 Statistics of weakly nonlinear waves on currents with strong vertical shear. *Phys. Rev. Fluids* **8** (1), 014801.